*Abstract
Click here to download Abstract: Abstract.docx

In-Plane Strengthening of Clay Brick Unreinforced Masonry Wallettes using ECC Shotcrete

Yi-Wei Lin[a]

[a] PhD Candidate, Department of Civil & Environmental Engineering, University of Auckland, New Zealand. Private Bag 92019, Auckland Mail Centre, Auckland 1142. ylin126@aucklanduni.ac.nz

Liam Wotherspoon[b]

[b] EQC Research Fellow, Department of Civil & Environmental Engineering, University of Auckland, Auckland, New Zealand. Private Bag 92019, Auckland Mail Centre, Auckland 1142. l.wotherspoon@auckland.ac.nz

Allan Scott[c]

[c] Lecturer, Department of Civil & Natural Resource Engineering, University of Canterbury, Christchurch, New Zealand. Private Bag 4800, Christchurch 8140, New Zealand allan.scott@canterbury.ac.nz

Jason M. Ingham[d]

[d] Associate Professor, Department of Civil & Environmental Engineering, University of Auckland, Auckland, New Zealand. Private Bag 92019, Auckland Mail Centre, Auckland 1142. New Zealand j.ingham@auckland.ac.nz

ABSTRACT

New Zealand’s stock of unreinforced masonry (URM) bearing wall buildings was principally constructed between 1880 and 1935, using fired clay bricks and lime or cement mortar. These buildings are particularly vulnerable to horizontal loadings such as those induced by seismic accelerations, due to a lack of tensile force-resisting elements in their construction. The poor seismic performance of URM buildings was recently demonstrated in the 2011 Christchurch earthquake, where a large number of URM buildings suffered irreparable damage and resulted in a significant number of fatalities and casualties. One of the predominant failure modes that occurs in URM buildings is diagonal shear cracking of masonry piers. This diagonal cracking is caused by earthquake loading orientated parallel to the wall surface and typically generates an “X” shaped crack pattern due to the reversed cyclic nature of earthquake accelerations.

Engineered Cementitious Composite (ECC) is a class of fiber reinforced cement composite that exhibits a strain-hardening characteristic when loaded in tension. The tensile characteristics of ECC make it an ideal material for seismic strengthening of clay brick unreinforced masonry walls. Testing was conducted on 25 clay brick URM wallettes to investigate the increase in shear strength for a range of ECC thicknesses applied to the masonry wallettes as externally bonded shotcrete reinforcement. The results indicated that there is a diminishing return between thickness of the applied ECC overlay and the shear strength increase obtained. It was also shown that, the effectiveness of the externally bonded reinforcement remained constant for one and two leaf wallettes, but decreased rapidly for wall thicknesses greater than two leafs. The average pseudo-ductility of the strengthened wallettes was equal to 220% of that of the as-built wallettes, demonstrating that ECC shotcrete is effective at enhancing both the in-plane strength and the pseudo-ductility of URM wallettes.

Keywords: Seismic; Masonry; Fiber Reinforced; Shotcrete; Strengthening

Click here to view linked References

1.0 Introduction

There are approximately 3800 unreinforced masonry (URM) bearing wall buildings in New Zealand, comprising a significant proportion of the nation's heritage building stock [1] with the majority of these URM buildings constructed between 1880 and 1935. As New Zealand is located at the boundary between the Australian Plate and the Pacific Plate, it is a country with high seismicity. Unfortunately, seismic forces were not appropriately considered when these URM buildings were originally constructed, and consequently this class of building typically lacks the tensile resisting structural elements that are necessary to sustain these seismic forces.

The earthquake vulnerability of New Zealand URM buildings has been clearly demonstrated in a number of previous earthquakes with the 1931 M7.8 Hawke's Bay earthquake [2] and more recently in the 2010 M7.1 Darfield earthquake [3-4] and 2011 M6.3 Christchurch earthquake [5-6] being responsible for causing the greatest extent of damage to URM buildings. The level of damage to URM buildings in these earthquakes included complete collapse (see Figure 1(a)), individual walls having completely or partially collapsed out-of-plane for earthquake loading oriented perpendicular to the wall (see Figure 1(b)); or varying levels of damage, including pier diagonal shear cracking, when earthquake loading was oriented parallel to the wall (see Figure 1 (c)).

While both in-plane and out-of-plane earthquake loading can cause significant damage to URM walls and piers, it is typically the wall characteristics in the in-plane direction that dictate the structural integrity of the complete building, as these walls are the structural elements that are required to transfer lateral earthquake forces into the foundation. URM bearing walls are typically composed of multi-leaf construction, with 2 and 3 leafs being the most common wall thickness, although single leaf thick walls are also observed, typically as part of cavity wall construction. Wall thicknesses exceeding 3 leaf are also encountered and tend to be used more commonly in URM buildings having a height exceeding two stories. Multiple in-plane failure modes exist for URM walls [8-10], with the type of failure exhibited by a wall being dependent on wall geometry, constituent material properties and the level of axial loading that the wall is subjected to. Of the multiple failure modes, four common in-plane failure modes are shown in Figure 2 [10]. The research reported here focused on the diagonal cracking failure mode, as this mode is regarded as being the most detrimental to the vertical load carrying capacity of a URM wall or pier [11].

Multiple techniques and products are available to improve the seismic performance of URM buildings, including, but not limited to: post-tensioning using steel reinforcing bars or strands; Near Surface Mounted

(NSM) reinforcement using steel reinforcing bars or Fiber Reinforced Polymer (FRP) strips; and surface bonded reinforcement such as shotcreting or FRP sheets [12-24].

Engineered Cementitious Composite (ECC) shotcrete is a cement composite that is reinforced with synthetic fibers. When loaded in tension, ECC exhibits a strain-hardening characteristic through the process of micro-cracking, where stresses are taken up by fibers that bridge the cracks. The strain-hardening characteristic of ECC makes it an ideal material for earthquake strengthening of URM buildings, as ECC can add both pseudo-ductility and strength to the building. Previous researchers [25-29] have tested URM elements strengthened with ECC and demonstrated significant improvements in ductility and strength when compared to the performance of the corresponding unstrengthened elements.

The study reported here investigated the effectiveness of ECC shotcrete as a seismic retrofitting technique to improve the in-plane response of URM walls with a separate study investigating the effectiveness of ECC shotcrete to improve the out-of-plane response of URM walls presented elsewhere [30]. The ECC mix proportions used are summarized in Table 1, which are similar to those used by previous researchers [31]. Preliminary investigations using the ECC mix adopted in this study indicated that a build thickness of 10 to 15 mm in a single spray can be achieved, so any specified shotcrete thickness in excess of 10 mm thick was applied successively in overlays of 10 mm, after the previously applied layers had hardened sufficiently.

2.0 Experimental Program

An experimental program was undertaken to investigate the effectiveness of sprayed ECC for in-plane strengthening of unreinforced clay brick masonry wallettes. Figure 3 diagrammatically summarized the scope of the test scheme, which was designed to determine both the strength increase as additional ECC overlays were applied, and the reduction in effectiveness of the externally bonded shotcrete as the wallette thickness increased. Two samples were tested for each geometric configuration, with the exception of the one ECC overlay applied on a two leaf wallette, where three samples were tested.

2.1 Wallette specimens

25 unreinforced masonry wallettes were constructed and tested, with the wallettes intentionally constructed in a manner that simulated the typical current condition of existing historical URM buildings. The wallettes were approximately 1.2 m high × 1.2 m long, with the thickness varying between 100 mm to 470 mm depending on the number of masonry leafs used. The vintage clay bricks used to construct the wallettes were recycled from demolished URM buildings and ASTM type O mortar was used with a cement: lime: sand ratio of 1:2:9 [32].

Researchers such as U. Andreaus, G. Ceradini and L. Ippoliti [8, 33-34] have recommended testing of masonry macro-elements such as wallettes for investigating the in-plane behavior of masonry walls.

It should also be noted that the experimental program was separated into two series, with series one having four wallettes and series two having 21 wallettes. The two series were constructed at different times but utilized identical mortar proportions and ECC mix ratios. The wallettes included in each series are reported in the next sub-section. The Common bond pattern was adopted, consisting of one header course after every four to six stretcher courses, as illustrated in Figure 4. Note that while the surface bond pattern for single leaf wallettes was identical to that for 2 and 4 leaf wallettes, the header courses were replaced by half bricks as it is not possible to include a header course for one leaf wallettes. Also, due to slight variations in brick dimensions, there were minor differences in the number of courses in each wallette (typically a wallette was 13±1 course in height). The compression strengths of the brick, mortar and masonry were determined using ASTM C67-00 [35], ASTM C109-09 [36] and ASTM C1314-00 [37] respectively, as reported in Table 2. Table 2 also summarizes the ECC material properties used in this study.

2.2 Implementation procedure

After the wallettes were built, the mortar was air cured for 28 days and then ECC shotcrete was sprayed onto those wallettes that were to be strengthened. Prior to spraying, the wallette surfaces were water blasted to both remove loose material and to pre-wet the surface. Polystyrene planks were then attached to the sides of the wallettes, to serve as an indicator of the thickness of ECC that needed to be sprayed. The ECC shotcrete was supplied in bagged form and added to a two stage mixer (see Figure 5(a)) from which the mixed material was pumped through a hose and sprayed onto the masonry wallettes (see Figure 5 (b)). An interval of approximately 45 minutes was provided between the applications of each successive ECC layer, which allowed the previously applied layer to harden. Each sprayed layer was trowelled flat so that the following layer of ECC was applied onto a flat surface (see Figure 5 (c)). Once spraying was completed, the polystyrene planks were removed and a constant water mist was applied onto the ECC shotcrete until the testing date.

The full testing configuration is shown in Table 3, with the wallette configurations designated using the code SX-YL-Z, where X, Y and Z represent the thickness of ECC overlay applied in mm, the number of leafs in the wallette thickness and the specimen number for this configuration, respectively. For example, S30-1L-2 represents a 30 mm ECC overlay applied on a single leaf thick masonry wallette, with the wallette being the second specimen with this configuration. Table 3 also reports the wallettes contained in each series.

2.3 Test setup

Wallette testing was conducted 14 days after spraying of the ECC overlay, using a modified version of the ASTM E519-07 test method [38]. The same modified method was used previously in studies to investigate the in-plane response of masonry wall sections extracted from existing URM buildings [39], and the response of laboratory strengthened wallettes [20, 22]. A schematic of the test setup is illustrated in Figure 6. Two steel loading shoes were placed on two diagonally opposite corners of the wallette, and were connected using two high-strength steel rods oriented along the wallette diagonal. A hydraulic actuator was attached to the top loading shoe to apply a diagonal compression load to the wallette. The load exerted on the wallette was measured by a load cell positioned between the hydraulic actuator and the top loading shoe. Two potentiometers were attached to the wallette to measure the diagonal displacements when the wallette was subjected to load.

3.0 Experimental results and discussions

Of the 25 wallettes tested, measurements were obtained successfully for 23 wallettes, with the displacement response for S10-2L-1 not recorded due to data interference but the shear stress measured. Measurements were not obtained for S30-3L-2 due to the recording software experiencing an unexpected error.

The diagonal compression force (P) applied to the wallette was converted into shear stress (τ) using Equation 1, where α is the angle between the horizontal axis of the wallette and the diagonal load applied, equal to 45 degrees in this test. t, H and B represent the thickness, height and length of the wallette respectively. The displacements measured by the two potentiometers were converted into horizontal drift using Equation 2, where ΔS and ΔL are the diagonal shortening and elongation of the wallette respectively, as measured by potentiometers placed parallel and perpendicular to the diagonal compression load. g represents the gauge length measured by each potentiometer.

$$\tau = \frac{P \cos \alpha}{0.5t(H+B)} \tag{1}$$

$$\delta = \frac{\Delta S + \Delta L}{2g}(\tan \alpha + \cot \alpha) \tag{2}$$

The shear stress-drift response of the tested wallettes is shown in Figure 7. Note that the figures showing the strengthened wallette response also include the corresponding as-built response. The maximum shear stress, ratio of strengthened and as-built strength, pseudo-ductility and shear modulus are presented in Table 4. These factors are described in the following sections.

3.1 General response of tested wallettes

The as-built wallette test results are presented in Figure 8, showing the measured average stress results as well as the measured stress from each individual wallette. The in-plane response of each individual as-built wallette is presented in Figure 7 (a,c,i,k). All as-built wallettes had similar response characteristics, with an almost linear relationship up to peak stress, followed by the formation of a diagonal stepped crack along the mortar joints, which resulting in a steep decline in the stress. The stress then remained relatively constant as the cracked upper section of the wallettes slid along the horizontal mortar joints of the stepped diagonal crack. All strengthened wallettes had similar response characteristics, increasing linearly up to the first cracking stress. The stress level resisted by the wallette then remained relatively constant as cracks developed and the stress was transferred and distributed across the ECC overlay. Final failure occurred when the ECC overlay debonded from the masonry surface. Representative crack patterns of the as-built and strengthened wallettes are shown in Figure 9. As-built wallettes typically exhibited a single diagonal crack after testing, while the strengthened wallettes exhibited multiple cracks spread over an area of the wallette surface, oriented in the direction of the load path.

3.2 Shear strength

As the thickness of the as-built wallette thickness increased, the peak shear stress that the wallette sustained did not remain constant (see Figure 8), and instead there was a significant decrease in the peak shear stress with increased thickness. This inconsistency in peak shear stress was most likely due to slight variation in the transfer of the applied load through the loading shoe as the wallette thickness increased. Therefore, comparisons of results have been made between wallettes of equal thickness and not across wallettes of varying thicknesses.

All strengthened wallettes showed an increase in maximum strength when compared with their unstrengthened counterparts. The overall increase in strength was between 130% and 469% (see Table 4). Figure 10 compares the strength increase with number of ECC overlays applied on a two leaf wallette, showing that as additional ECC overlays were applied, the ratio of strength increase to number of ECC overlays decreased. Figure 10 indicated that any ECC overlay with a thickness in excess of 30 mm will provide a diminishing return in terms of the strength increase of the wallette.

A factor K_{wt} was defined to represent the variable effectiveness of ECC due to wall thickness, where wt represents wall thickness. The measured K_{wt} factors from the testing are shown in Table 5, where values have been normalized against two leaf thick wallettes that are used as the reference thickness in this study because that is the most commonly used wall thickness in NZ URM buildings. The K_{wt} factor remains relatively constant between one and two leaf wallettes, with one leaf having a slightly lower value of 0.9, most likely caused by the variation in the ECC shotcrete strength. The K_{wt} factors decreased significantly for three and four leaf wallettes, indicating that there was not sufficient physical or chemical bonds between the different leafs of the wallette to ensure they behaved in unison under load. Therefore, it is recommended for design purposes that either additional wall connections should be installed for walls exceeding two leafs in thickness, or the appropriate K_{wt} factor should be applied to reduce the design capacity accordingly.

Since the critical failure mode was debonding, the equation developed by the Japan Concrete Institute (JCI) [40] to predict FRP bond failure to concrete was modified to predict ECC bond strength to vintage clay brick masonry. The shear bond strength ($V_{\tau ECC}$) is calculated using Equation 3, where f'_b is the brick compression strength in MPa and E_{ECC} is the Young's modulus of ECC, also in MPa. A_{Bond} represents the bond area in m^2, and due to the diagonal crack that splits the wallette into two approximately equal areas, is equal to half of 1.2 m × 1.2 m in this study. The values of K_{wt} have been previously summarized in Table 5 and M is a function that describes the saturated increment in shear strength provided when additional ECC overlay is applied. M is calculated using Equation 4, where t_{ECC} denotes the thickness of ECC in meters. Figure 11 demonstrates the correlation between the strengths calculated using Equation 3 and the actual testing results, with a regression coefficient of 92.2% indicating a good agreement between the two.

$$V_{\tau ECC} = K_{wt} \times 0.12 f'_b \times E_{ECC} \times M \times A_{Bond} \tag{3}$$

$$M = 0.0033\,(1 - e^{-92 t_{ECC}}) \tag{4}$$

3.3 Pseudo-ductility

Previous research has demonstrated that masonry walls are capable of energy dissipation and can behave in a ductile manner when subjected to lateral forces [41-43]. However, the non-linear behavior of masonry walls results in difficulty when quantifying the structural ductility. This difficulty arises from the ambiguity of defining a distinct yield point when considering the associated force-displacement response. To overcome this difficulty, multiple researchers have suggested the use of bilinear idealization of the masonry force-displacement response [44-45], where the total hysteretic energy dissipated is identical for the bilinear idealization and the original force-displacement curve. With a bilinear idealization of the masonry wall response, adopting the ductility value as the ratio of the ultimate displacement to yield displacement (of the bilinear idealization) is accepted in various publications [44-47] and such ductility is referred to as pseudo-ductility.

Equation 5 was used to determine the pseudo-ductility of the wallettes in this study, where μ represents the pseudo-ductility, δ_u is the ultimate drift and is defined as the point where the strength had degraded to 80% of the peak strength, and the yield drift δ_y was determined from a bilinear response that had energy absorption equivalent to the measured in-plane response. For scenarios where the strength did not degrade below 80% of the peak strength prior to wallette failure, the ultimate drift was defined as the drift value at the failure strength. The adopted definition and calculation method for determining pseudo-ductility was also used by numerous researchers [47-51] when calculating the ductility of masonry wallettes.

$$\mu = \frac{\delta_u}{\delta_y} \tag{5}$$

The calculated pseudo-ductility (Table 4) showed that as-built wallettes had a mean value of 2.4 with a coefficient of variation (CoV) of 66%, while the strengthened wallettes had a mean pseudo-ductility of 5.2 and a CoV of 52%. The CoV of both as-built and strengthened wallettes indicate a high variability in pseudo-ductility, which was partially attributed to the stress redistribution that occurs prior to peak load. However, despite the large variability, the strengthened wallettes on average exhibited a 220% increase in pseudo-ductility over the as-built wallettes, demonstrating the additional energy absorption that was achieved with strengthening.

3.4 Shear modulus

The shear modulus (also known as modulus of rigidity), G, is the ratio of the shear stress to shear strain, measured as the secant modulus between 5-70% of τ_{max} in the τ-δ curve along the initial loading arm prior to τ_{max}. The calculated G values are presented in Table 4, from which the elastic modulus (E) was derived using Equation 6, where □ is the Poisson's ratio and is assumed to be 0.25, identical to that used in [22].

$$E = 2G(1 + \upsilon) \tag{6}$$

The strengthened wallettes exhibited lower stiffness than their as-built counterparts, which was partially caused by minor cracking and deformation of the masonry elements as they transferred stresses to the ECC overlay during the loading stage. It was also observed that the strengthened wallettes exhibited a tendency to warp in the out-of-plane direction due to uneven stiffness between the strengthened and unstrengthen surfaces, which also contributed to the lower stiffness.

3.5 Design procedure

Based on the results obtained in this study, the following design procedures are proposed for in-plane strengthening of masonry walls using ECC.

1. Determine the expected in-plane failure mode and the design shear force of the wall using an appropriate guideline such as [47]. If the expected failure mode is diagonal cracking, proceed to the next step, otherwise alternative strengthening techniques is required.
2. Assume the total thickness of ECC that will be applied over the wall surface (either on a single surface or both surfaces) and calculate the shear strength of the ECC section (V_{ECC}) according to Equation 7, as reproduced from Japan Society of Civil Engineers (JSCE) [52], where t_{ECC} is the thickness of the ECC overlay in mm and f'_{tECC} the ECC tensile strength in MPa. z is the moment lever arm distance in mm and taken as 0.72 of the wall length that ECC will be applied to, exclusive of any wall length that crosses wall openings. If V_{ECC} exceeds the design shear force, proceed to the next step, otherwise increase the ECC overlay thickness and recalculate the section shear strength.

$$V_{ECC} = t_{ECC} \times z \times f'_{tECC} \tag{7}$$

3. Determine the shear bond strength ($V_{\tau ECC}$), calculated using Equation 3 with an appropriate bond area (doubled if ECC is to be applied on both surfaces). If the shear bond strength exceeds the design shear force then the design is complete, otherwise additional connections will be required to increase the bond strength and alternative equations should be adopted to calculate the new bond strength.

4.0 Conclusions

Testing was conducted on 25 masonry wallettes to determine the effectiveness of in-plane strengthening using sprayed ECC. The study investigated the influence on strength gain of the number of ECC overlays applied as well as the reduction of strength gain from applied ECC overlays when the thickness of the wallette increased. The following conclusions were made:

1. All strengthened wallettes had increased shear strength over their as-built counterparts, with this strength increase being between 130% and 514%. As more ECC overlay was applied, the additional strength increase provided by each additional ECC overlay decreased.
2. The effectiveness of the ECC overlay were similar between one leaf and two leaf wallettes, but

decreased as the wallette thickness increased to three and four leafs. It is recommended that in design, wall connections should be installed for walls that are more than two leafs, or the appropriate K_{wt} factor be adopted to reduce the design capacity.

3. All strengthened wallettes had a significantly higher pseudo-ductility than their as-built counterparts, with an average increase of 220% times over the as-built wallettes. The stiffness of strengthened wallettes was found to be lower than that of as-built wallettes, which indicates that there is no increase in stiffness with the application of ECC shotcrete.
4. A three step design procedure on strengthening masonry walls using ECC is provided based on the results of this study as well as equations derived by Japan Society of Civil Engineers.

Acknowledgements

The authors thank Derek Lawley, David Nevans, Richard Leary, Gareth Williams and Mason Pirie from Reid Construction Systems for the funding and assistance in producing the ECC samples, and thank Matt Pronk from Vijay Frame & Truss for providing the space for storage and testing of the wallette specimens. The authors also thank Florine Rimeur, Aurelien Credoz and Jeremie Baudet for their assistance in testing the wallette samples. Lastly the authors thank the New Zealand Ministry of Science and Innovation for the funding of Yi-Wei Lin’s doctoral study.

References

1. Russell A P, Ingham J M**.** Prevalence of New Zealand's unreinforced masonry buildings. Bulletin of the New Zealand Society for Earthquake Engineering 2010; 43 (3): 182-201.
2. Dowrick D J. Damage and intensities in the magnitude 7.8 1931 Hawke's Bay, New Zealand, Earthquake. Bulletin of the New Zealand National Society for Earthquake Engineering 1994; 31(3):139-62.
3. Dizhur D, Ismail N, Knox C, Lumantarna R, Ingham J M. Performance of unreinforced and retrofitted masonry buildings during the 2010 Darfield Earthquake. Bulletin of New Zealand Society of Earthquake Engineering 2010; 43(4): 321-39.
4. Ingham, J M & Griffith, M. Performance of unreinforced masonry buildings during the 2010 Darfield (Christchurch, NZ) Earthquake, Australian Journal of Structural Engineering 2011; 11(3): 1-18.
5. Moon L, Dizhur D, Griffith M & Ingham, J M. Performance of unreinforced clay brick masonry buildings during the 22nd February 2011 Christchurch Earthquake. Structural Engineering Society (SESOC) Journal 2011; 24(2): 59-84.
6. Ingham J M, Biggs D T & Moon L M. How did unreinforced masonry buildings perform in the February 2011 Christchurch Earthquake? Structural Engineer 2011; 89(6): 1-12.
7. Smith S C. Earthquake destruction in Hastings. 1931. Wellington, Alexander Turnbull Library, reproduced with permission.
8. Andreaus U & Ceradini G. Failure modes of solid brick masonry under in-plane loading. Masonry International 1992; 6(1): 4-8.
9. Andreaus U. Failure criteria for masonry panels under in-plane loading. Journal of Structural Division-ASCE 1996; 122(1): 37-46.
10. Magenes G & Calvi G M. In-plane seismic response of brick masonry walls. Earthquake Engineering & Structural Dynamics 2007; 26(11): 1091-112.
11. Bruneau M. State-of-the-art report on seismic performance of unreinforced masonry buildings. Journal of Structural Engineering 1994; 120(1): 230-51.

12. ElGawady M, Lestuzzi P & Badoux M. A review of conventional seismic retrofitting techniques for URM. In: 13th International Brick and Block Masonry Conference. Amsterdam, Netherlands; 2004. p. 1-10.
13. Yang K, Joo D, Sim J, Kang J. In-plane seismic performance of unreinforced masonry walls strengthened with unbonded prestressed wire rope units. Engineering Structures 2012; 45: 449-459.
14. Ma R, Jiang L, He M, Fang C, Liang F. Experimental investigations on masonry structures using external prestressing techniques for improving seismic performance. Engineering Structures 2012; 42: 297-307.
15. Turco V, Secondin S, Morbin A., Valluzzi M R & Modena C. Flexural and shear strengthening of un-reinforced masonry with FRP bars. Composites Science and Technology 2006; 66(2): 289-96.
16. Grande E, Milani, G & Sacco E. Modelling and analysis of FRP-strengthened masonry panels. Engineering Structures 2008; 30(7): 1842-60.
17. Hamed E & Rabinovitch. Failure characteristics of FRP-strengthened masonry walls under out-of-plane loads. Engineering Structures 2010; 32(8): 2134-45.
18. Willis C, Seracino, R & Griffith M. Out-of-plane strength of brick masonry retrofitted with horizontal NSM CFRP strips. Engineering Structures 2010; 32(2): 547-55.
19. Valluzzi M R, Tinazzi D & Modena C. Shear behavior of masonry panels strengthened by FRP laminates. Construction and Building Materials 2002; 16(7): 409-16.
20. Mahmood H & Ingham J M. Diagonal compression testing of FRP-retrofitted unreinforced clay brick masonry Wallettes. Journal of Composites for Construction 2011; 15: 810-20.
21. Konthesingha K, Masia M, Petersen R, Mojsilovic N, Simundic G, Page A. Static cyclic in-plane shear response of damaged masonry walls retrofitted with NSM FRP strips – An experimental evaluation. Engineering Structures 2013; 50: 126-136.
22. Ismail N, Petersen R B, Masia M J & Ingham J M. Diagonal shear behaviour of unreinforced masonry wallettes strengthened using twisted steel bars. Construction and Building Materials 2011; 25(12): 4386-93.
23. Goodwin C, Tonks G & Ingham J. M. Retrofit techniques for seismic improvement of URM buildings. Journal of the Structural Engineering Society of New Zealand 2011; 24(1): 30-45.
24. Dizhur D, Derakhshan, H, Lumantarna R, Griffith M & Ingham J M. Out-of-Plane Strengthening of

Unreinforced Masonry Walls Using Near Surface Mounted Fibre Reinforced Polymer Strips. Journal of the Structural Engineering Society of New Zealand 2010; 23(2): 91-103.

25. Kim Y Y, Kim J S, Ha G J & Kim J K. Influence of ECC Ductility on the Diagonal Tension Behaviour (Shear Capacity) of Infill Panels. In: Proceedings of the International RILEM Workshop on High Performance Fiber Reinforced Cementitious Composites in Structural Engineering. Honolulu, Hawaii Island, USA; 2005. p. 403-10

26. Kyriakides M. A. & Billington S L. Seismic retrofit of masonry-infilled non-ductile reinforced concrete frames using sprayable ductile fiber-reinforced cementitous composites. The 14th World Conference on Earthquake Engineering. Beijing, China; 2008. p. 1-7.

27. Maalej M, Lin V W J, Nguyen M P & Quek S T. Engineered cementitious composites for effective strengthening of unreinforced masonry walls. Engineering Structures 2010; 32(8): 2432-9.

28. Mechtcherine V, Bruedern A-E. & Urbonas T. Strengthening/retrofitting of masonry by using thin layers of sprayed strain-hardening cement-Based composites (SSHCC), 4th International Conference on Concrete Repairs. Dresden, Germany: 2011. p. 451-60.

29. Bruedern A-E, Abecasis D & Mechtcherine V. Strengthening of masonry using sprayed strain hardening cement-based composites (SHCC). Seventh International RILEM Symposium on Fibre Reinforced Concrete: Design and Applications. Chennai (Madras), India: 2008. p. 451-60.

30. Lin, Y. W., Lawley, D., Wotherspoon, L. & Ingham, J. M. Seismic Retrofitting of an Unreinforced Masonry Building Using ECC Shotcrete, New Zealand Concrete Industry Conference. Wellington, New Zealand: 2011. p. 1-9.

31. Kim Y, Kong H-J & Li V. Design of engineered cementitious composite suitable for wet-mixture shotcreting. ACI Materials Journal 2003; 100(6): 511-8.

32. American Society for Testing and Materials. ASTM-C270-08a: Standard Specification for Mortar for Unit Masonry: 2008.

33. Andreaus, U & Ippoliti, L. A two-storey masonry wall under seismic loading: a comparison between simple and strengthened masonry. In: ERES 96, 1st International Conference on Earthquake Resistant Engineering Structures. , Vol. 2, Thessaloniki, Greece; 1996. p. 561-70.

34. Andreaus U & Ippoliti L. Masonry panels under in-plane loading: a comparison between experimental and numerical results, In: CMEM 95, 7th International Conference on "Computational Methods and Experimental Measurements". Capri, Italy; 1995. p. 603-10.

35. American Society for Testing and Materials. ASTM-C67-00: Standard Test Methods for Sampling and Testing Brick and Structural Clay Tile. Masonry test methods and specifications for the building industry: 2000.

36. American Society for Testing and Materials. ASTM-C-109/C-109M-99: Standard Test Method for Compressive Strength of Hydraulic Cement Mortars (using 2-in or 50-mm cube specimens). Masonry test methods and specifications for the building industry: 2009.

37. American Society for Testing and Materials. ASTM-C-1314-00a: Standard Test Method for Compressive Strength of Masonry Prisms. Masonry test methods and specifications for the building industry: 2001.

38. American Society for Testing and Materials. ASTM-E519-02: Standard Test Method for Diagonal Tension (Shear) in Masonry Assemblages. Masonry test methods and specifications for the building industry: 2002.

39. Dizhur D, Lumantarna R, Derakhshan H & Ingham J M. Earthquake-damaged unreinforced masonry building tested in-situ. Structural Engineering Society (SESOC) Journal 2011; 23(2): 76-89.

40. Japan Concrete Institute. Technical Report of Technical Committee on Retrofit Technology. In: International Symposium on Latest Achievement of Technology and Research on Retrofitting Concrete Structures. Kyoto, Japan; 2003. p. 1-8.

41. Magenes G & Calvi G. In-plane seismic response of brick masonry walls. Earthquake Engineering & Structural Dynamics 1998; 26(11): 1091:112.

42. Griffith, M C, Vaculik J, Lam N T K, Wilson J, Lumantarna E. Cyclic testing of unreinforced masonry walls in two-way bending. Earthquake Engineering & Structural Dynamics 2007; 36(6): 801-21.

43. Sucuoglu H & Erberik A. Performance evaluation of a three-storey unreinforced masonry building during the 1992 Erzincan Earthquake. Earthquake Engineering & Structural Dynamics 1997; 26(3): 319-36.

44. Park, R. Evaluation of ductility of structures and structural assemblages from laboratory testing. Bulletin of the New Zealand National Society for Earthquake Engineering 1989; 22(3): 155-166.

45. Tomazevic, M. Earthquake-resistant design of masonry buildings London: Imperial college press; 1999.

46. CEN. 1998-1: Eurocode 8–Design of Structures for earthquake resistance–Part 1: General rules, seismic actions and rules for buildings: 2004.

47. Ingham, J. M. (Ed.) Assessment and Improvement of Unreinforced Masonry Buildings for Earthquake Resistance (February 2011 Draft version). University of Auckland, Faculty of Engineering. Auckland, New Zealand: 2011.

48. Prota, A, Marcari, G, Fabbrocino, G, Manfredi, G and Aldea, C. Experimental in-plane behaviour of tuff masonry strengthened with cementitious matrix–grid composites. Journal of Composites for Construction 2006; 10(3): 223-233.

49. Marcari, G, Manfredi, G, Prota, A, and Pecce, M. In-plane shear performance of masonry panels strengthened with FRP. Composites, Part B 2007; 38(7–8): 887–901.

50. Ismail, N, Petersen, R B, Masia, M J and Ingham, J M. Diagonal shear behaviour of unreinforced masonry wallettes strengthened using twisted steel bars. Construction and Building Materials 2011; 25(12): 4386-4393.

51. Mahmood, H and Ingham J Diagonal compression testing of FRP-retrofitted unreinforced clay brick masonry wallettes. Journal of Composites for Construction 2011; 15(5): 810-820.

52. Japan Society of Civil Engineers. Recommendations for Design and Construction of High Performance Fiber Reinforced Cement Composites with Multiple Fine Cracks (HPFRCC). Japan: 2008.

Table 1
ECC mix proportions used in this study

Materials	Kg/m^3
Sand	640
Cement	800
Fly ash	240
Water	374
Fiber	26
Additives	0.3

Table 2
Masonry and ECC material properties used in this study

Masonry Material		
Series 1		
f'_b (N/mm^2)	f'_j (N/mm^2)	f'_m (N/mm^2)
26.5	0.8	6.6
Series 2		
f'_b (N/mm^2)	f'_j (N/mm^2)	f'_m (N/mm^2)
16.3	1.0	5.3
ECC material		
f'_t (N/mm^2)	f'_c (N/mm^2)	
3	40	

Table 3
Summary of wallette testing configurations

Wallette configuration	Wallette dimension (mm)			Thickness of ECC overlay (mm)	Number of samples
	Height	Length	Thickness (leaf)		
S0-1L[2]	1200	1200	100 (1)	0	2
S30-1L[2]	1200	1200	100 (1)	30	2
S0-2L[1]	1200	1200	220 (2)	0	2
S10-2L[1]	1200	1200	220 (2)	10	3
S20-2L[1]	1200	1200	220 (2)	20	2
S30-2L[1]	1200	1200	220 (2)	30	2
S40-2L[2]	1200	1200	220 (2)	40	2
S50-2L[2]	1200	1200	220 (2)	50	2
S0-3L[2]	1200	1200	350 (3)	0	2
S30-3L[2]	1200	1200	350 (3)	30	2
S0-4L[2]	1200	1200	470 (4)	0	2
S30-4L[2]	1200	1200	470 (4)	30	2

[1] The first sample of this configuration belongs to series 1 with the rest belonging to series 2
[2] All samples of this configuration belongs to series 2

Table 4

Summary of results from wallette testing

Wallette configuration	Sample Number	P_{max} (kN)	F_{max} (kN)	τ_{max} (N/mm^2)	τ_{max}/τ_{o1} (%)	δ_y (%)	δ_u (%)	μ	$G \times 10^3$ (N/mm^2)	$E \times 10^3$ (N/mm^2)
S0-1L	1	27.4	19.4	0.16	N/A	0.5	1.7	1.0	1.8	4.4
	2	27.3	19.3	0.16	N/A	1.6	1.6	3.6	2.0	5.0
S30-1L	1	140.8	99.6	0.75	468.8	0.4	3.7	9.4	0.1	0.3
	2	140.6	99.4	0.75	468.8	2.8	11.8	4.2	0.2	0.5
S0-2L	1	30.2	21.3	0.07	N/A	0.2	0.8	4.8	3.5	8.8
	2	29.7	21.0	0.09	N/A	0.5	0.5	1.0	4.5	11.2
S10-2L	1	67.2	47.5	0.18	186.0	N/A				
	2	130.9	92.5	0.35	362.1	3.1	15.4	5.0	0.6	1.3
	3	81.9	57.9	0.21	226.7	6.2	24.0	3.7	0.1	0.3
S20-2L	1	123.2	87.1	0.33	341.0	0.1	1.4	10.5	0.09	0.2
	2	104.6	73.9	0.28	289.3	3.9	7.5	1.9	0.02	0.06
S30-2L	1	179.2	126.7	0.48	496.0	1.2	4.9	4.2	0.04	0.11
	2	139.2	98.4	0.35	385.1	0.8	3.2	3.2	0.3	0.8
S40-2L	1	156.1	110.4	0.45	432.0	0.8	6.5	8.5	0.3	0.8
	2	148.4	104.9	0.32	410.7	4.6	13.3	2.9	0.03	0.07
S50-2L	1	116.8	82.6	0.28	323.2	0.6	4.6	8.0	1.4	3.5
	2	186.8	131.3	0.56	514.0	3.2	11.1	3.5	0.05	0.1
S0-3L	1	55.7	39.4	0.09	N/A	0.4	0.4	1.0	5.9	14.8
	2	46.1	32.6	0.09	N/A	1.2	3.4	2.8	0.4	1.1
S30-3L	1	95.1	67.2	0.15	186.9	6.8	15.9	2.4	0.04	0.1
	2	N/A								
S0-4L	1	50.1	35.4	0.07	N/A	0.5	0.5	1.0	5.5	13.7
	2	69.4	49.1	0.08	N/A	0.4	1.6	3.9	0.5	1.3
S30-4L	1	95.9	67.8	0.11	160.4	3.7	26.0	7.0	0.5	1.4
	2	77.8	55.0	0.09	130.2	1.4	5.7	4.0	0.1	0.3

Where P_{max} = maximum applied diagonal force; F_{max} = maximum horizontal shear force; τ_{max} = maximum shear stress, τ_{max}/τ_{o1} = ratio of max shear stress to as-built wallette; δ_y = % drift at yield; δ_u = % drift at failure; μ = pseudo-ductility; G = shear modulus and E = modulus of elasticity

Table 5
K_{wt} factor to account for effectiveness of ECC as wall thickness increases

Wall thickness (leaf)	K_{wt} factor
1	0.9
2	1.0
3	0.6
4	0.5

(a) Damage caused by the 1931 M7.8 Hawke's Bay earthquake, [reproduced from 7]

(b) Collapse of out-of-plane loaded URM walls in the 2010 M7.1 Darfield earthquake

(c) In-plane diagonal cracks caused by the 2011 M6.3 Christchurch earthquake

Figure 1: Examples of damage to New Zealand URM buildings as a result of seismic loading

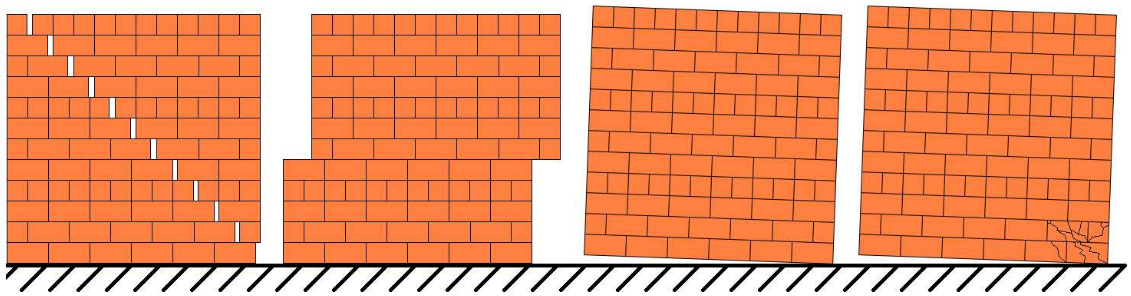

(a) Diagonal cracking (b) Shear sliding (c) Rocking (d) Toe Crushing

Figure 2: Masonry in-plane failure modes

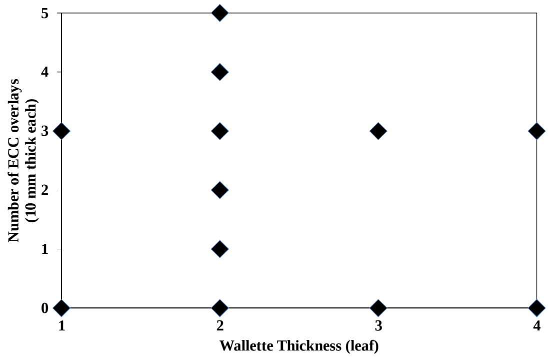

Figure 3: Test spectrum of range of wallette thickness and number of ECC overlays

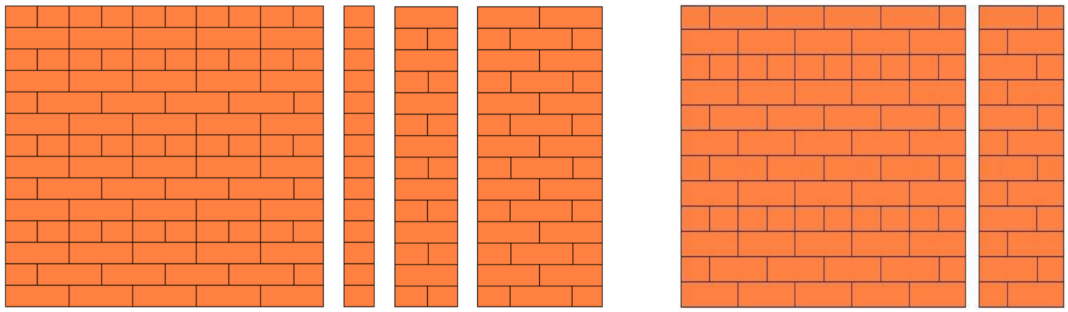

(a) Front and side view of 1, 2 and 4 leaf wallettes (b) Front and side view of 3 leaf wallette

Figure 4: Wallette bond patterns

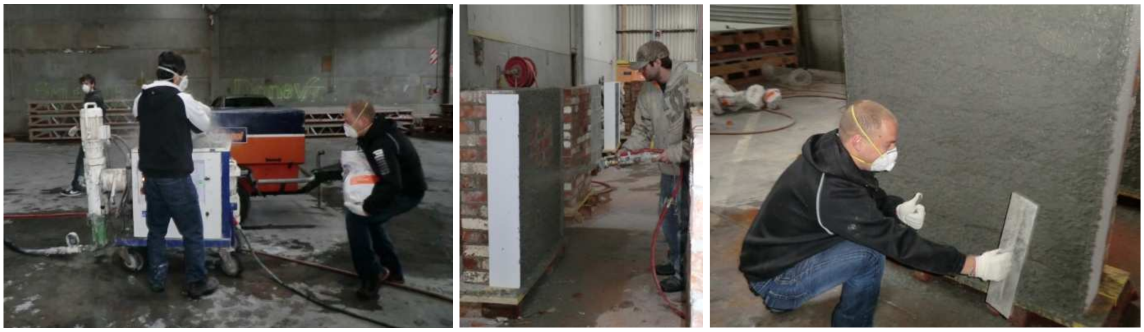

(a) Adding prebagged ECC into mixer (b) Spraying of ECC shotcrete onto wallette (c) Trowelling sprayed ECC flat prior to the spraying of successive layers

Figure 5: Images of the application of ECC onto the wallette specimens

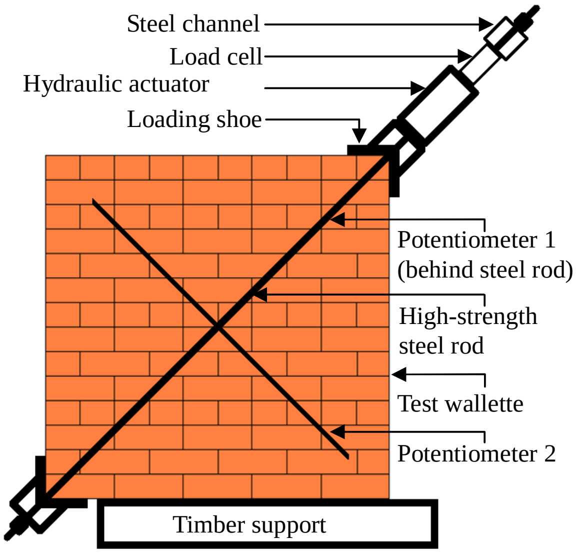

Figure 6: Modified wallette test setup

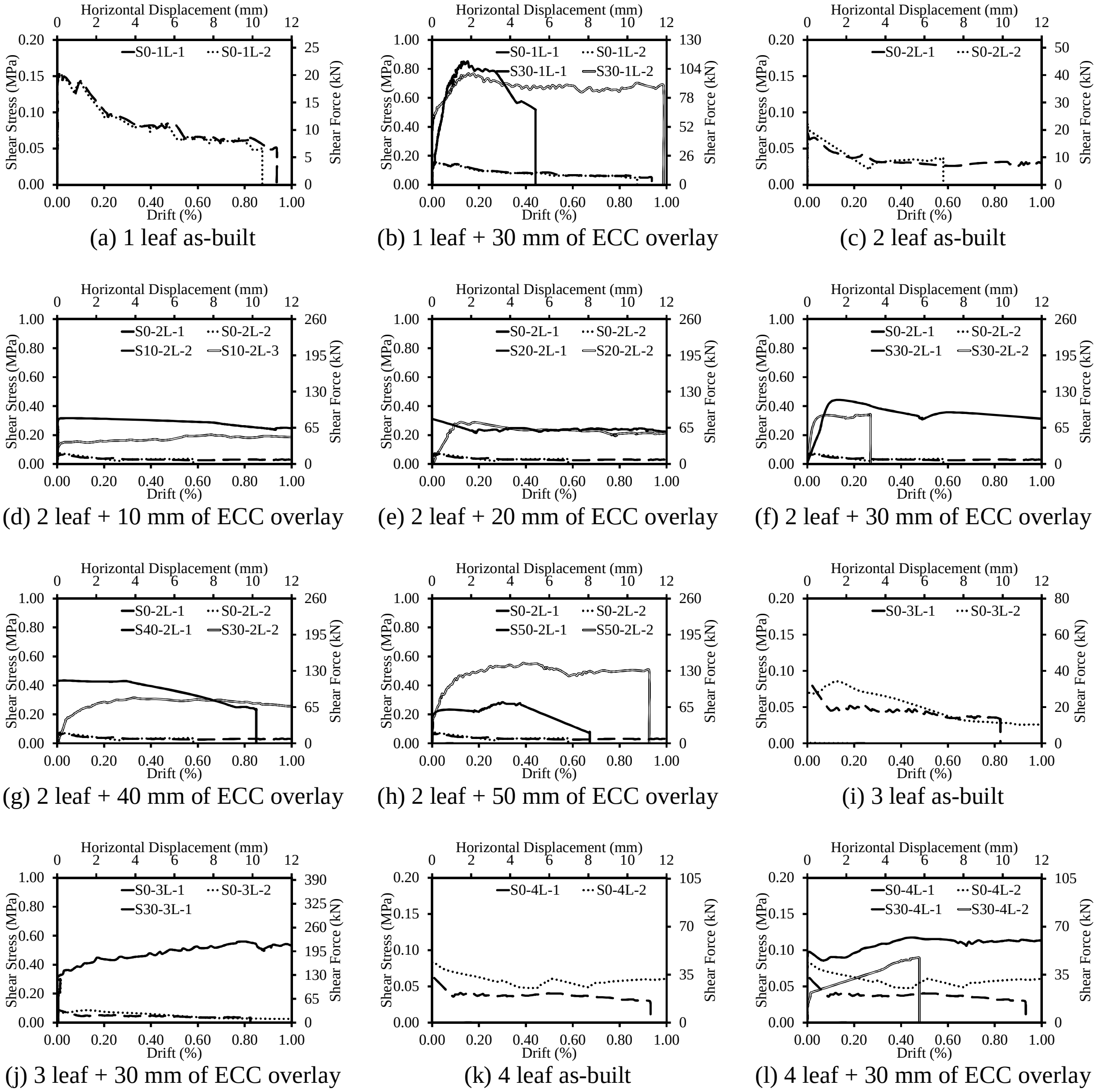

(a) 1 leaf as-built (b) 1 leaf + 30 mm of ECC overlay (c) 2 leaf as-built

(d) 2 leaf + 10 mm of ECC overlay (e) 2 leaf + 20 mm of ECC overlay (f) 2 leaf + 30 mm of ECC overlay

(g) 2 leaf + 40 mm of ECC overlay (h) 2 leaf + 50 mm of ECC overlay (i) 3 leaf as-built

(j) 3 leaf + 30 mm of ECC overlay (k) 4 leaf as-built (l) 4 leaf + 30 mm of ECC overlay

Figure 7: Shear stress-drift plots of tested wallettes

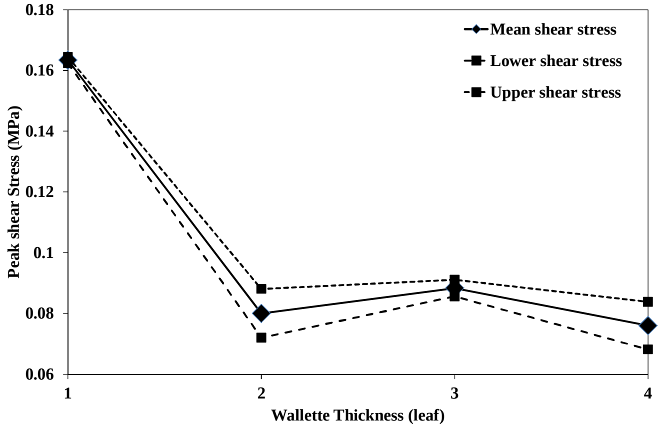

Figure 8: Peak shear stress of as-built wallettes

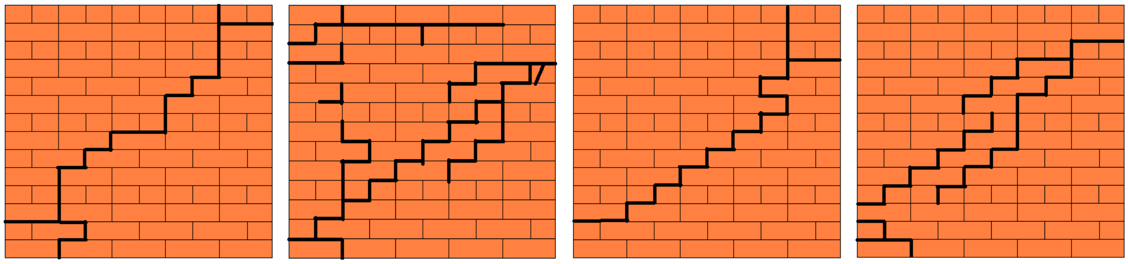

(a) As-built wallette (S0-2L-2) | (b) Strengthened wallette (S30-2L-2) | (c) As-built wallette (S0-4L-1) | (d) Strengthened wallette (S30-4L-2)

Figure 9: Examples of wallette crack patterns

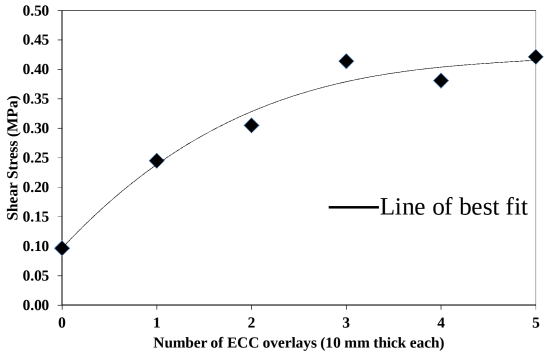

Figure 10: Peak shear stress for a number of ECC overlays applied to two leaf wallettes

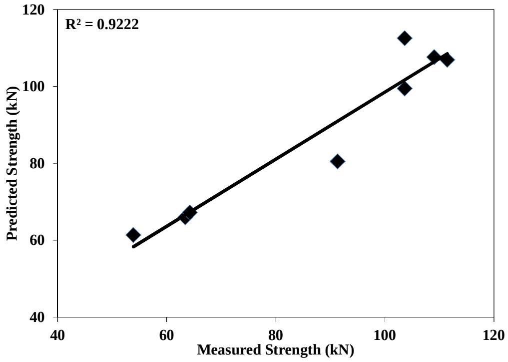

Figure 11: Correlation between predicted shear strength using modeled equations and measured strength results.